Article:
Wang, H, Xu, X, Wang, C orcid.org/0000-0002-4301-3974 et al. (2 more authors) (2021) Fundamental Insight into the Degradation Mechanism of an rGO-Fe3O4 Supercapacitor and Improving Its Capacity Behavior via Adding an Electrolyte Additive. Energy and Fuels, 35 (9). pp. 8406-8416. ISSN 0887-0624

https://doi.org/10.1021/acs.energyfuels.1c00653

Fundamental insight into the degradation mechanism of an rGO-Fe_3O_4 supercapacitor and improving its capacity behaviour via adding an electrolyte additive

Hai Wang[a,b], Xingping Xu[a], Chun Wang[b], Anne Neville[b] and Yong Hua [b]*

[a]: College of Mechanical and Electronic Engineering, China University of Petroleum (East China), Qingdao, 266555, China

[b]: Institute of Functional Surfaces, School of Mechanical Engineering, University of Leeds, Leeds, LS2 9JT, United Kingdom

*Corresponding author: Yong Hua, E-mail address: Y.Hua@leeds.ac.uk

Abstract

rGO-Fe_3O_4 nano-sized composites containing various concentrations of rGO(reduced Graphene Oxides) were synthesized by the hydrothermal method. rGO nanosheet provides a solid framework for Fe_3O_4, improving the overall conductivity as well as reducing agglomeration of Fe_3O_4 nanoparticles. rGO-Fe_3O_4 exhibits a specific surface area of 207.2 $m^3 g^{-1}$ with a total pore volume of 0.203 $cm^3 g^{-1}$. Fabricated into electrode, rGO-Fe_3O_4 demonstrates a specific capacitance of 182.2 $F \cdot g^{-1}$ at a current density of 1.25 $A \cdot g^{-1}$ with a retention rate maintaining at 92.4% after 1000 cycles. Material degradation of the electrode inevitably changes the solid electrolyte interface(SEI) and causes capacitance loss during long-cycle tests. In this regard, advanced surface analysis techniques were applied to better understand the degradation mechanism and reveal possible reactions occurring at the electrode interface after various cycling stages. Strategically, Iron molybdate($FeMoO_4$) has been added as an electrolyte additive in the experiment where molybdenum disulfide(MoS_2) formed on the electrode surface and remarkably rejuvenated the capacity with maximum values rising to 186.6 $F \cdot g^{-1}$, 171.8 $F \cdot g^{-1}$ and 153.4 $F \cdot g^{-1}$ at the current densities of 1.25 $A \cdot g^{-1}$, 2.50 $A \cdot g^{-1}$ and 3.75 $A \cdot g^{-1}$ respectively. The notable recovery of capacitance achieved by adding $FeMoO_4$ provides a practical method in solving the problem of material degradation and rejuvenating rGO-Fe_3O_4 electrode performance in Na_2SO_3-based electrolyte.

Keywords: rGO-Fe_3O_4, degradation mechanism, supercapacitor, interface

Introduction

As high-performance energy storage devices, supercapacitors have both fast charge-discharge characteristics and battery energy storage characteristics. They are a promising chemical power source and belong to the emerging class of power compensation and energy storage devices. Compared with conventional capacitors, the advantages of supercapacitors mainly include high power density, low cost, long cycle life, and high recyclability[1-3]. Supercapacitors have significant advantages in fast electronic transmission, promoting them widely used in electric vehicles, renewable energy power generation systems, rail transportations and aerospace applications.

Transition metal oxide (TMOs) such as NiO, Co_3O_4, and TiO_2 have shown remarkable capability in electrochemical performance and electric capacitance [4-6]. In addition, TMO nano-structured compounds combined with graphene, carbon nanotubes, fullerenes have attracted attention in the field of energy storage [7-9]. Among them, nanosized magnetite (Fe_3O_4) exhibits potentially attractive properties in applications such as high-efficiency energy storage devices and supercapacitors with high specific capacitance. In order to solve the problem of the low conductivity and the agglomeration of Fe_3O_4 nanoparticles strategically, carbon-based materials (such as graphene) are commonly used to improve the electrochemical properties of Fe_3O_4 electrode in an aqueous environment due to the low dynamic viscosity of aqueous electrolytes [10-13]. The rGO-Fe_3O_4 composites prepared by Jianling [14] can reach a high specific capacity of 1065 mAh•g-1 at a current density of 0.1 A•g-1. The prepared rGO-Fe_3O_4 carbon (AC) lithium-ion capacitor has an excellent energy density of 98.8 Wh•kg-1 and a power density of 3.4 kW•kg-1. However, it retained 78.9% after 1000 charge/discharge cycles; the degradation mechanism causing this large performance drop is unclear.

Understanding the degradation mechanism of the electrode and inhibiting material degradation is particularly challenging. Krzysztof [15] described the degradation mechanisms at the interface between the carbon-Li_2SO_4/$LiNO_3$ electrolytes using Raman spectroscopy. In their system, material degradation was caused by the oxidation of the carbon surface or reduction of the negative ions. Masahiro [16] studied the aging characteristics of carbon electrodes and the results showed that the Faradaic process on the negative electrode is the main cause of the decrease of capacitance. Muhammad [17] demonstrated the successful surface engineering of polyaniline coated iron oxide nanoparticles (Fe_3O_4/PANI-NPs), with PANI coating preventing degradation of the material as well as improving the capacitance stability from 92% to 96.5% at current density of 15 A g^{-1} after 25,000 charge-discharge cycles. Abbas [18] demonstrated that the MoO_4^{2-} anion improved the total capacitance and inhibited corrosion based on the Faradaic process, and Na_2MoO_4 has been considered as the additive in a 1 mol•L^{-1} lithium sulfate electrolyte. Chodankar [19] applied redox-active electrolytes to multi-wall Carbon nanotubes/manganese dioxide (MWCNTs/MnO_2) and achieved a significant improvement in electrochemical performance in a redox-induced Na_2SO_4 electrolyte, with a maximum specific capacitance of 1012 F•g^{-1} at the current density of 2 mA•cm^{-2}. Mingyuan [20] improved the capacitance of an activated carbon electrode from 147.1 F•g^{-1} to 229.2 F•g^{-1} (1A•g^{-1}) by adding 0.1 M $K_3Fe(CN)_6$ in 2M KOH electrolyte. Although there are many published studies considering the electrochemical performance and application prospects of Fe_3O_4 related composites in supercapacitor, none of them have revealed the fundamental degradation mechanism of Fe_3O_4 electrode. Therefore, it is of great significance to understand the material deterioration occurs on the Fe_3O_4 electrode surface scientifically.

In this work, Fe_3O_4 nanoparticles (Fe_3O_4 NPs) were successfully grown on the graphene nanoplate via a simple hydrothermal route, which created a large specific surface area. However, capacity deterioration was found over long-term charge/discharge processes. Therefore, this work has two goals; firstly, to reveal the material deterioration mechanism of the rGO-Fe_3O_4 composites as a candidate supercapacitor over long-term charge/discharge processes. Secondly, to improve the capacitance by introducing iron (II) molybdate ($FeMoO_4$) as an additive. This work correlated the electrochemical measurements, specific capacities, and long-term stability with the detailed surface morphology changes, Furthermore, the introduced $FeMoO_4$ as an additive has rejuvenated the specific capacitance, simultaneously providing a feasible solution to mitigate capacity loss and extend the service life of supercapacitors.

Materials and methods

Material preparation

Iron (III) chloride hexahydrate ($FeCl_3 \cdot 6H_2O$) was purchased from VWR Chemicals (USA). Sodium acetate (NaAc), sodium dodecyl sulfate (SDS), polyethylene glycol (PEG) and $FeMoO_4$ were purchased from Sigma-Aldrich, Ethylene glycol (EG) was purchased from Fisher Scientific (UK). Sodium sulfite was bought from Alfa Aesar and graphene nanoplates were purchased from SUZHOU TANFENG GRAPHENE TECHNOLOGY Co., Ltd. All the chemicals were used as received without further purification.

Synthesis of Fe_3O_4 NPs

Fe_3O_4 NPs were synthesized by the hydrothermal method [21-22]. 2.7g $FeCl_3 \cdot 6H_2O$ was dissolved in a 100ml ethylene glycol and put on a hotplate with magnetic stirring for 25 minutes. Then 7.2 g NaAc and 2.0 g of SDS were slowly added into the solution for another stirring of 15 minutes. In the next step, the mixture solution was transferred into a Teflon-based autoclave with a nitrogen flow for 30 minutes to remove oxygen and then hydrothermally treated at 190 °C for 8h. After the mixture was cooled to room temperature, Fe_3O_4 NPs were collected by an external magnetic method in order to remove the impurities, and then followed by washing several times with ethanol and deionized water. Finally, the products were dried under vacuum at 100 °C for 12 h.

Synthesis of rGO- Fe_3O_4 composites

To prepare rGO-Fe_3O_4 composites containing various mass ratios of rGO, a rGO suspension was prepared by adding a certain amount of rGO to deionized water (20 mL) and sonicating for 30 minutes to form a suspension (suspension I). Meanwhile, 2.7 g of prepared Fe_3O_4 NPs and 2 g of PEG were dissolved in 60 ml of ethylene glycol with 200 mg sodium dodecylbenzene sulfonate (SDBS) and the mixture solution was stirred at 60°C for an hour (suspension II). Suspension I was then added to suspension II and mixed uniformly, and the homogeneous mixture was transferred to a polytetrafluoroethylene-based autoclave and deoxygenated with nitrogen for an hour followed by heating to the desired temperature of 190 °C for 12 hours. The products were washed with ethanol and deionized water at least three times. They were then extracted by using magnetic separation and dried overnight in a constant temperature oven at 70°C. Final products are labeled as 0.75 $mg \cdot ml^{-1}$-rGO-Fe_3O_4, 1.5 $mg \cdot ml^{-1}$-rGO-Fe_3O_4 and 3.0 $mg \cdot ml^{-1}$-rGO-Fe_3O_4 respectively, according to the mass of rGO within rGO-Fe_3O_4 composites, which was measured by thermal gravimetric analysis (TGA, Mettler Toledo Star^e System). It can be noted that the small increase in carbon content when rGO concentration doubles may be attributed to the uneven dispersion of rGO in the aqueous environment [23].

The morphology of the products was observed by scanning electron microscopy (SEM, FESEM, Hitachi SU8230), the crystal structure of the composites was obtained using (XRD, Panalytical X'pert Pro) and Raman spectroscopy. The elemental composition of the products was characterized by Electron energy-dispersive x-ray spectroscopy (EDS, Oxford AZtec). N_2 adsorption-desorption was carried out by TriStar 3000 V6.04 to obtain data for pore-size distribution, isothermal desorption and specific surface area (SSA).

Electrochemical characterization of rGO-Fe_3O_4 supercapacitor

Electrochemistry tests were conducted in a standard three-electrode system. The electrolyte is 1 mol/L Na_2SO_3 solution with platinum foil as the counter electrode and a saturated

silver/silver chloride as the reference electrode. cyclic voltammetry (CV) and electrochemical impedance spectroscopy (EIS) tests were performed at room temperature using an ACM Gill 1800 electrochemical workstation. For the rGO-Fe_3O_4 electrode, cyclic voltammetry was performed at a potential range of -1.2 V and 0.15 V versus silver/silver chloride. The AC impedance test frequency ranged from 100 kHz to 10 mHz. The galvanostatic charge/discharge tests (GCD) at various current densities were performed using a LAND CT-2001A battery test system (Wuhan Jinnuo Electronics Co., Ltd.).

The specific capacitance is calculated according to the following equation [24-26]:

$$C = I\frac{\Delta t}{m\Delta V} \quad (1)$$

Where C ($F \cdot g^{-1}$) is the specific capacitance, I(A) represent the discharge current, m(g), ΔV(V) and Δt (s) represent the mass of the active materials, the potential drop during discharge and the total discharge time, respectively.

Fabrication of a supercapacitor electrode

The prepared active material, acetylene black (carbon black, acetylene 99%, Alfa Aesar) and polyvinylidene fluoride (PVDF, Alfa Aesar) were mixed at a weight ratio of 8:1:1 and thoroughly mixed to a uniform slurry which was spread on an aluminum foil and dried for 12 h at 100 °C in a vacuum oven. After drying, 10 MPa pressure was applied to the electrode, thereby improving the stability and electrochemical performance of the electrode. Afterward, the electrode was cut into a square chip (area=1 cm × 1 cm). Specifically, the loading amounts of rGO-Fe_3O_4 were determined by comparing the weight of aluminum foil.

Results and discussion

The SEM images of Fe_3O_4 NPs, graphene nanoplates and rGO-Fe_3O_4 composites are provided in Figure 1(a), (b) and (c). The synthesized Fe_3O_4 NPs displayed a similar diameter of 100 nm. The SEM images of the rGO-Fe_3O_4 composites exhibit a two-dimensional sheet morphology with the Fe_3O_4 NPs attached to the wrinkled surface of graphene, this observation was in good agreement with previous works [27-28]. The knitted coupling between the Fe_3O_4 NPs and graphene is derived from thermodynamically stable bending, and high conductivity graphene provided efficient and rapid electron transport for the charge storage. The overall Raman results of graphene, pure Fe_3O_4, and rGO-Fe_3O_4 samples are shown in Figure 1(d). The characteristic peak of Fe_3O_4 appeared at 675 cm^{-1}. The D band around 1343 cm^{-1} is attributed to the presence of chaotic graphite structures caused by amorphous carbon and defects, which stems from the symmetric A1g model of defective graphite. The G band near 1571 cm^{-1} is derived from the tangential in-plane tensile vibration of the C-C band, which is attributed to the E_2g graphite model [29-31]. In addition, the intensity of the G-band is stronger than the intensity of the D-band, and the intensity ratio of the D-band and G-band (ID/IG) is used to evaluate the degree of modification or defect of the rGO [32]. The Raman results confirmed that the prepared rGO-Fe_3O_4 composites have a lower ID/IG ratio, exhibiting an ordered crystalline structure with the presence of fewer structural defects [33-35]. The overall XRD pattern for the reduced graphene oxide(rGO), pure Fe_3O_4 NPs, and rGO- Fe_3O_4 composites are shown in Figure 1(e). It is clear that the peaks at 2θ of 18.3°, 30.1°, 35.4°, 43.1°, 56.9°, 62.5° and 74.5 corresponded to (2 2 0), (3 1 1), (4 0 0), (5 1 1), (4 4 0) and (5 3 3) were well matched with a typical Fe_3O_4 spinel phase (JCPDS no. 19-0629) [36]. Four distinctive peaks at 26°, 44.5°, 54.3° and 65° were observed for crystalline graphite, confirming the presence of rGO-Fe_3O_4 composites were synthesized successfully via the hydrothermal method [37]. SSA and total pore volume (TP) results obtained

by N_2 adsorption-desorption are provided in Figure 1(f), both of which increase with increasing rGO concentrations and reach a maximum of 207.2 $m^3 g^{-1}$ and 0.203 $cm^3 g^{-1}$. TGA analysis shows the mass fraction (wt.%) of rGO within the samples were 12.2%, 15.7%, and 18.5%, respectively, suggesting that the increase in the rGO concentration can provide high conductivity and sufficient active sites for charge storage and ion diffusion.

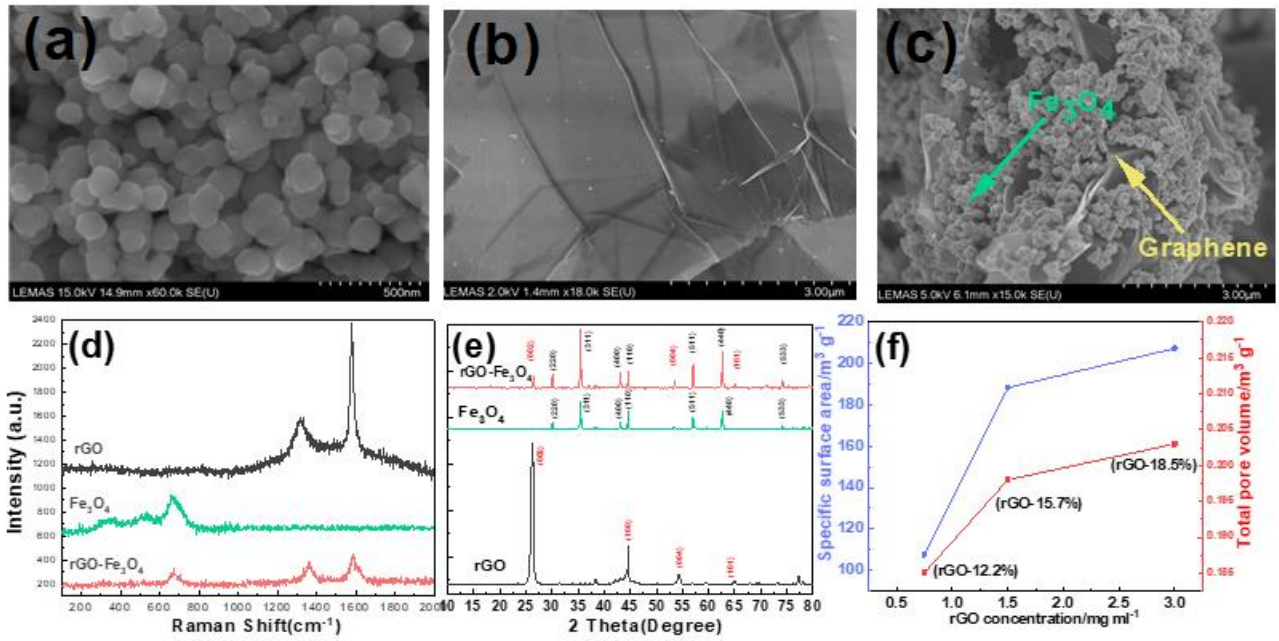

Figure 1 (a) Fe_3O_4 NPs, (b) rGO nanoplates, (c) rGO-Fe_3O_4 composites (d) Raman spectroscopy of graphene, Fe_3O_4 NPs and rGO-Fe_3O_4 composites (e) XRD patterns of rGO, Fe_3O_4 NPs, and rGO- Fe_3O_4 composites (f) specific surface area and total pore volume of rGO-Fe_3O_4 with different rGO concentrations

Electrochemical properties and capacitance characteristics of rGO-Fe_3O_4 material were investigated by cyclic voltammetry tests in a 1M Na_2SO_3 solution. Figure 2(a) shows that the rGO-Fe_3O_4 composite electrode has a voltage window of -1 V to 0.15 V at various scan rates of 2.5 $mV{\bullet}s^{-1}$, 5 $mV{\bullet}s^{-1}$, 10 $mV{\bullet}s^{-1}$, 20 $mV{\bullet}s^{-1}$, 30 $mV{\bullet}s^{-1}$, and 50 $mV{\bullet}s^{-1}$, respectively. The CV curves exhibit that the characterization of the capacitance is different from an ideal electric double layer capacitance (EDLC). The results also show that the shape remains the same at various scan rates, the areas of CV curves were bigger as the increased in the scan rates, suggesting that rGO-Fe_3O_4 has fast diffusion at the material interface with high capacitive behaviour. The CV curve shows two coupled redox peaks near -1 V and -0.2 V, indicating the presence of Fe_3O_4 NPs provides favorable surface adsorption sites for sulfite anions, which acts as the subsequent catalyst for redox or intercalation reactions. Energy storage of supercapacitors mainly depends on the pore size of the electrode material and their relationship with the solvated ion size of electrolyte [38]. Possible reactions to the sulfur-containing product are listed in Equations 2 and 3 [39]. Similar work was done by Shih-Yu [40], where the main reaction mechanisms for the current system, rGO-Fe_3O_4 composites exposed to the Na_2SO_3 solution is the redox reaction of sulfur from sulfate and sulfite anions or the intercalation of sulfite ions for the redox reaction between Fe^{2+} and Fe^{3+}.

$$2SO_3^{2-} + 3H_2O + 4e^- \leftrightarrow S_2O_3^{2-} + 6OH^- \quad (2)$$

$$S_2O_3^{2-} + 3H_2O + 8e^- \leftrightarrow 2S^{2-} + 6OH^- \quad (3)$$

The AC impedance spectra of pure Fe_3O_4 NPs and rGO-Fe_3O_4 composites with various rGO concentrations are shown in Figure 2(b). The three impedance spectra of various rGO concentrations have similar features, a semicircle at the high-frequency region and a Warburg impedance represented the diffusion of ions in the bulk electrode. As the rGO concentrations rose from 0.75 mg•ml^{-1} to 3.0 mg•ml^{-1}, R_{ct} values decreased from 2.08 Ω to 1.62 Ω, suggesting that the enhanced conductivity and high-capacity performance. The straight line obtained in the low-frequency region is attributed to the Warburg impedance and the electrode with an rGO content of 3.0 mg•ml^{-1} has a small capacitive reactance, which is attributed to the acceleration of electron transport and reduction of resistance by rGO. The pure Fe_3O_4 NPs electrode has the largest semicircle in the high-frequency range, suggesting a higher charge-transfer resistance of the electrode.

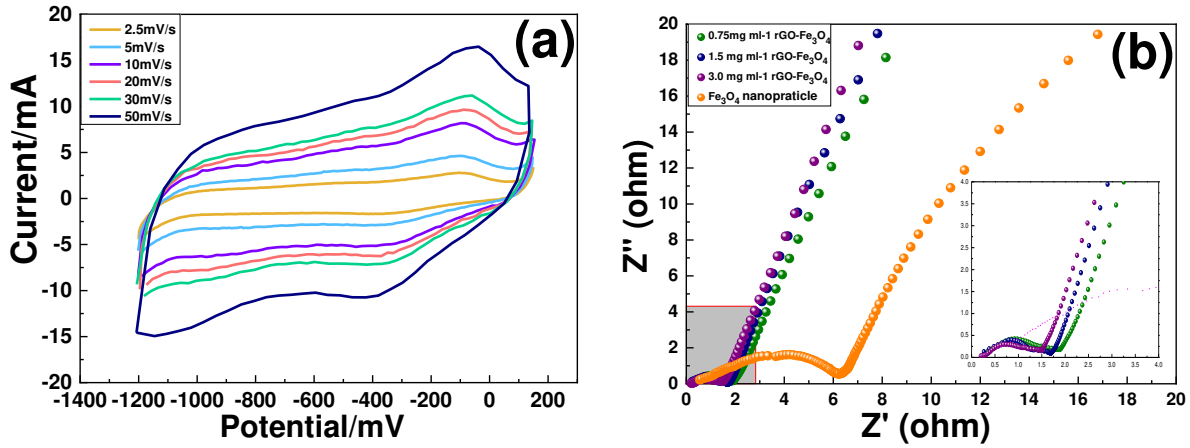

Figure 2(a) Cycling voltammetry of rGO-Fe_3O_4 composite with an rGO concentration of 1.5mg•ml^{-1} measured by a potential varying from -1.2 V to 0.15 V; (b) Nyquist plots of rGO-Fe_3O_4 composites in a 1 M Na_2SO_3 electrolyte with various rGO concentration compared with pure Fe_3O_4

The capacitance behaviour of rGO-Fe_3O_4 composites containing various rGO was further studied by GCD tests at various current densities and shown in Figure 3. The geometrically symmetrical triangular curves in Figure 3(a) verify the behaviour of an ideal pseudocapacitor and the highly reversible charge-discharge process [41]. At low current density, the passivation zone occurred before the point reached 0.15 V during the charging process, and the results showed that the increase in current densities, resulted in the charge and discharge time being reduced. According to Figure 3(b), specific capacitances of 212.8 F•g^{-1}, 182.5 F•g^{-1}, 151.4 F•g^{-1}, 130.5 F•g^{-1} and 122.1 F•g^{-1} were recorded for rGO-Fe_3O_4 composites at the corresponded current densities of 0.75 A•g^{-1}, 1.25 A•g^{-1}, 2.5 A•g^{-1}, 3.75 A•g^{-1}, 5 A•g^{-1}, respectively, indicating that the reduction of the specific capacitance was observed, and suggesting a low current density having better accessibility of ions go into the electrode material. The long-term cycle performance of 1.5 mg•ml^{-1}-rGO-Fe_3O_4 composites at current densities of 0.75 A•g^{-1} and 5 A•g^{-1} is provided in Figure 3(c). The results indicate a better retention rate of 92.4% at 0.75 A•g^{-1} compared with 87.7% at the current density of 5 A•g^{-1}. Moreover, the results also suggest that the specific capacitance of rGO-Fe_3O_4 improves significantly with the increase in the rGO concentrations from 0.75 mg•ml^{-1} to 1.5 mg•ml^{-1} as shown in Figure 3(d). Compared to the pure Fe_3O_4 NPs, the enhanced electrochemical performance was partly attributed to the good electronic conductivity of graphene [42]. In Figure 3(d), as the rGO concentration increased from 0.75 mg•ml^{-1} to 1.5 mg•ml^{-1}, higher rGO concentration provides high conductivity and sufficient active sites for charge storage and ion diffusion, thus enhancing the electrodes' charge-discharge performance and the specific capacitance is significantly improved from 126.2 F•g^{-1} to 212.8 F•g^{-1} at the current density of 0.75

A•g^{-1}. When rGO concentration was further increased from 1.5 mg•ml^{-1} to 3.0 mg•ml^{-1}, however, the excessive rGO was covered the Fe_3O_4 nanoparticles and hinder the interaction with the electrolyte, thereby reducing the capacitance to 188.1 F•g^{-1}, similar observation has been reported by Yanqun [43].

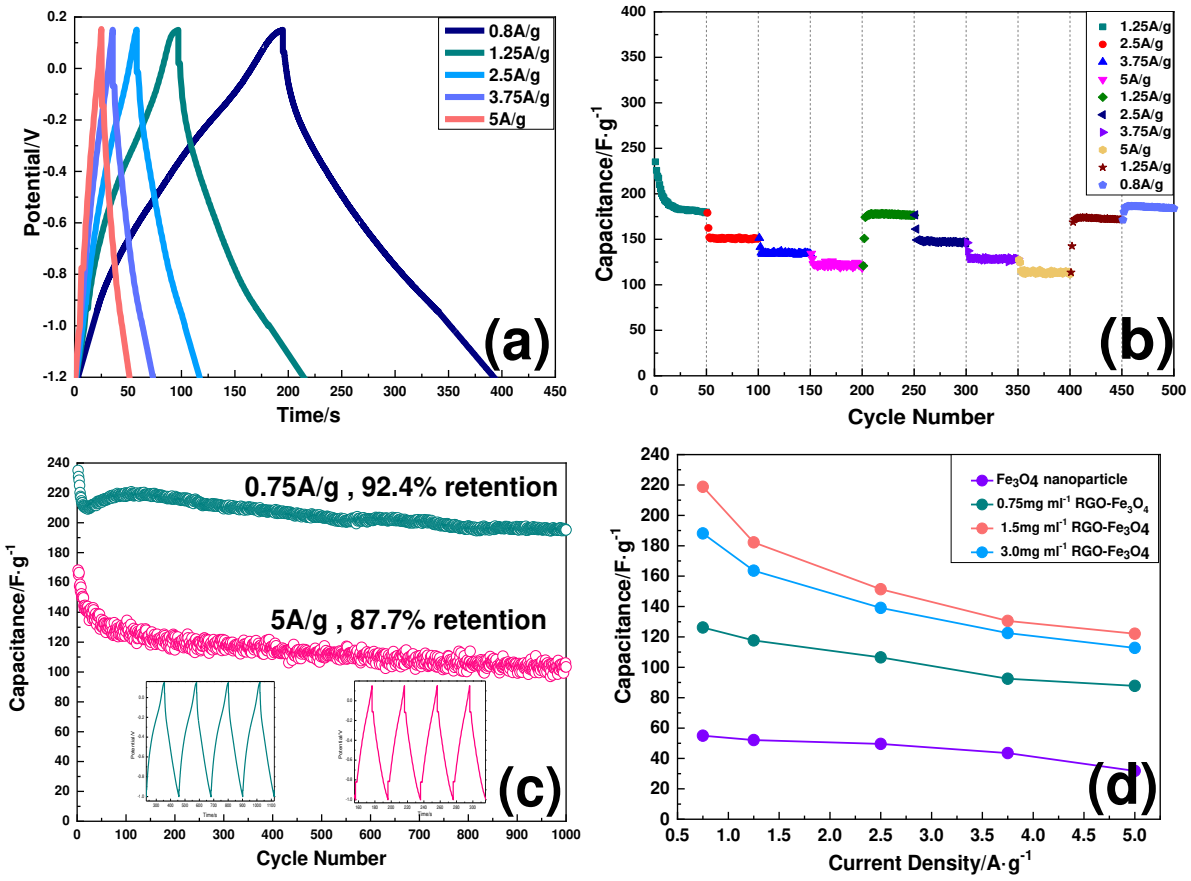

Figure 3(a) GCD curves of rGO-Fe_3O_4 composite with an rGO concentration of 1.5 mg•ml^{-1} at various current density (b) Cycling performance (c) Long-term coloumbic efficiency and capacity retention at the current densities of 0.75 A•g^{-1} and 5 A•g^{-1} and (d) Specific capacitance of samples with different rGO concentration at various current densities.

The morphology of the electrode surface after GCD at a constant current of 1.25 A•g^{-1} in a 1 M Na_2SO_3 solution was observed by SEM. The development of the corrosion products was observed during the charge and discharge processes as shown in Figure 4(a). It can be seen from Figure 4(b) that the rGO-Fe_3O_4 composites started to form clusters of spherical particles with sizes ranging from 100 nm to 500 nm. After 500 cycles, the corrosion products covered the entire electrode surface as shown in Figure 4(c). By comparing the XRD spectra before and after the cycling tests, peaks appeared at 2θ =29.7°, 33.6°, 43.2° and 53.2° were detected, which corresponded to (1 1 0), (1 1 2), (1 1 4) and (3 0 0) of FeS(JCPDS no. 65-3356) as shown in Figure 4(d). It should be noticed that the characteristic peaks at 2θ =38 °, 44°, 65°and 78 ° are derived from the aluminum foil during electrode fabrication. Therefore, it can be concluded that FeS was determined to be the reaction product that may cause the capacitance deterioration.

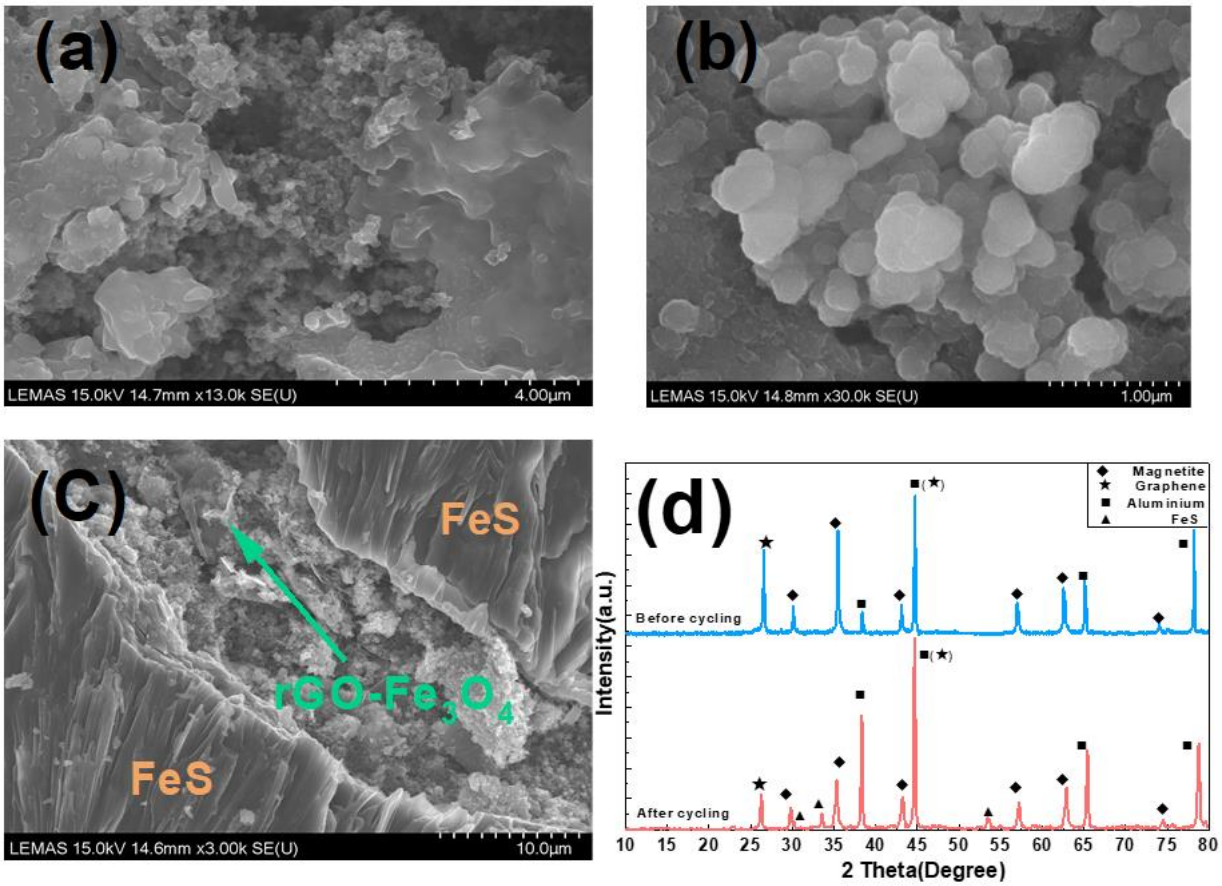

Figure 4 (a),(b),(c)The formation of FeS on the electrode surface (d) XRD patterns before and after the GCD measurements

The effect of $FeMoO_4$ as an electrolyte additive on the capacitance performance

The rGO-Fe_3O_4 composites were further surface engineered to improve the capacity performance during the charge and discharge processes at different current densities via introducing $FeMoO_4$ as an additive to the electrolyte. $FeMoO_4$ was added to the 1M Na_2SO_3 electrolyte and mixed well to form a homogeneous mixture. Figure 5 shows the change of the capacitance after introducing 500mg $FeMoO_4$. It is interesting to note that the capacitance started to increase after 200 cycles and the highest peaks were detected at 475 cycles, 492 cycles and 497 cycles with a capacity of 187 $F \cdot g^{-1}$ 172 $F \cdot g^{-1}$ and 153 $F \cdot g^{-1}$ for the current densities of 1.25 $A \cdot g^{-1}$, 3.75 $A \cdot g^{-1}$ and 5 $A \cdot g^{-1}$, respectively. The scattered particles in Figure 5(b) show reaction products grow on the rGO-Fe_3O_4 electrode surface after 200 cycles and suggest that the formation of the products was able to increase the electrical conductivity and effectively improve the capacity performance.

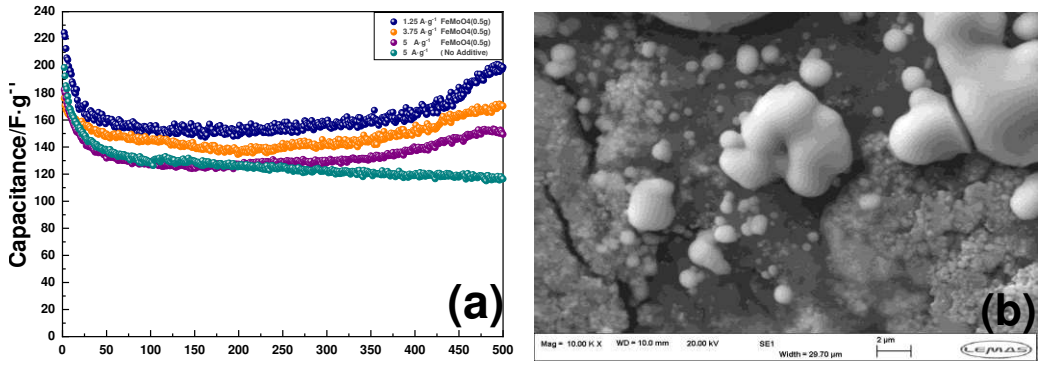

Figure 5(a) Comparison of specific capacitance after adding Iron(II) Molybdate with no additive, (b) morphology of growing MoS_2

In order to investigate the function of the flaky products formed on the surface and their role in renewing the capacitance of the rGO-Fe_3O_4 electrode, both electrochemistry experiments and surface analysis were performed. We observed the growth of flaky products after 500 cycles on the electrode surface via SEM images as shown in Figures 6(a) and 6(b).

EDS analysis, XRD and Raman spectroscopy were used to identify the surface products formed on the electrode surface. The EDS results in Figure 6(c) show a uniform elemental distribution of Mo, S, O, Fe and C within the products. XRD peaks in Figure 6(d) at 2θ = 14.2°, 33.1°, 39.2° and 58.9° were assigned to (0 0 2), (1 0 0), (1 0 3) and (1 1 0), corresponding to MoS_2 [44] (JCPDS card no. 37-1492). Figure 6 (b and c) indicates that the presence of MoS_2 was determined and the results suggest that the formation of MoS_2 and rGO-Fe_3O_4 composites were detected on the electrode surface after various charge/discharge cycles. Raman spectroscopy in Figure 6(e) clearly shows the two characteristic peaks at 380.7 cm^{-1} and 407.8 cm^{-1}, which correspond to the E^1_{2g} and A_{1g} mode of MoS_2 respectively. The separation between the two peaks of 26.3 cm^{-1} is larger than the 19 cm^{-1} reported for exfoliated flakes [45-47]. Combined with the rejuvenating capacitance during the charge and discharge described in Figure 5(a), generated MoS_2 builds a structure of staggered gaps and channels instead of covering the entire surface, which allows electrical interaction between rGO-Fe_3O_4 and the electrolyte and effectively improves the capacitive performance.

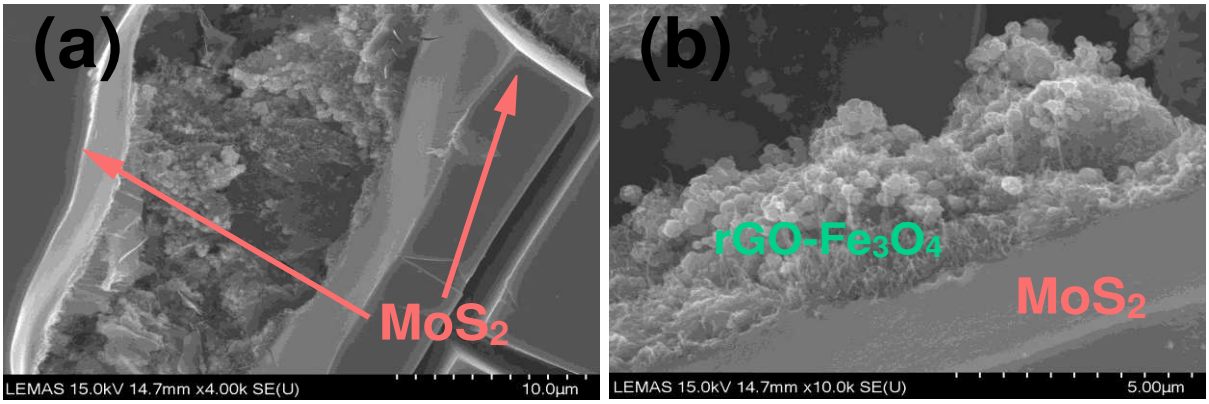

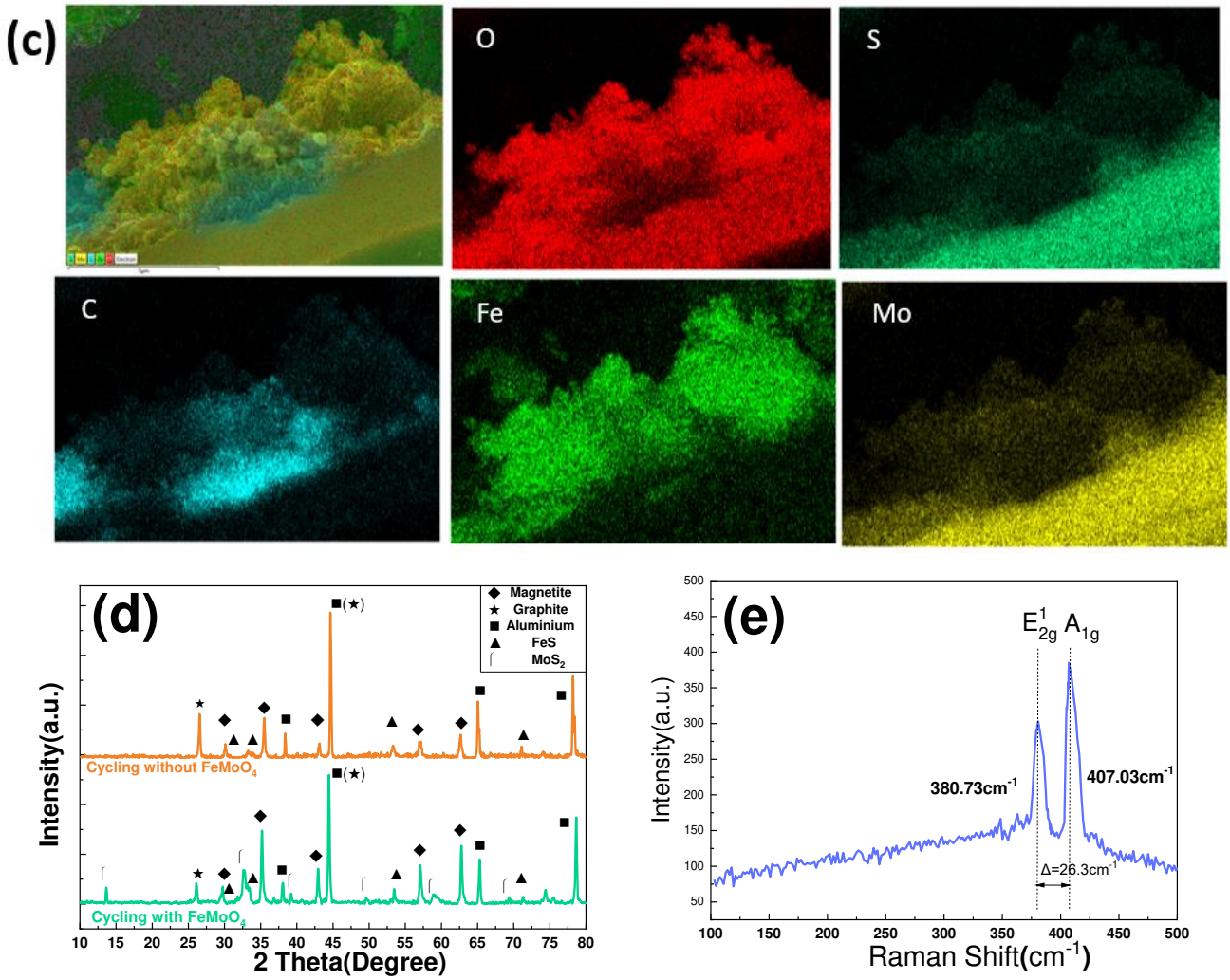

Figure 6(a)SEM images of the flaky MoS_2, (b)MoS_2 with rGO-Fe_3O_4 composites (c)EDS mapping of the MoS_2 with rGO-Fe_3O_4 composites, (d) Compared XRD pattern of the electrode after cycling and (e)Raman spectroscopy of MoS_2

In order to clarify that the observation of the formation of MoS_2 increases the capacity performance through introducing the $FeMoO_4$ to the electrolyte during the charge and discharge processes, cyclic voltammetry and AC impedance of the electrode in the mixed electrolyte at specific cycles of 100, 300, 500 were tested at a current density of 1.25 $A \cdot g^{-1}$. Cyclic voltammetry in Figure 7(a) shows that the redox peak near -0.1 V gradually weakens, indicating the deteriorating of the redox reaction of divalent iron ions. An enhanced oxidation peak appeared near -1.0 V, corresponding to the formation of flaky MoS_2 on the electrode surface. Cycling voltammetry was consistent with the XRD and Raman results. The EIS measurements in Figure 7(b) provides the electrochemical behaviour of the material after various cycles in terms of electrolyte resistance and charge transfer resistance. The results showed that the materials after the 100^{th} cycle exhibited a bigger semicircle at the high-frequency region compared to the 500^{th}, indicating that the electron transfer resistance reduced from 1.95 Ω to 1.52 Ω, suggesting the improved conductivity and ion transport for the formation of MoS_2 on the rGO-Fe_3O_4 electrode.

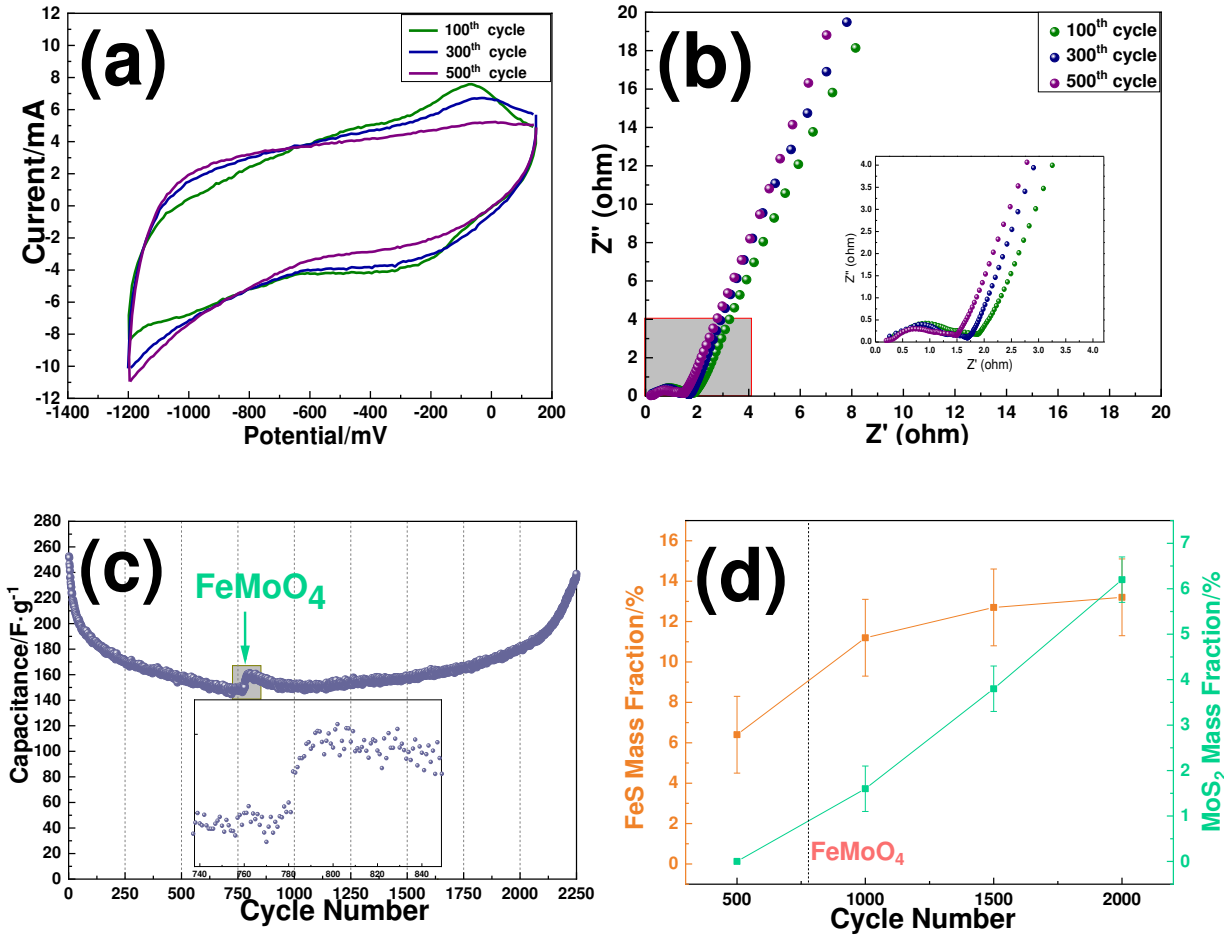

Figure 7(a) CV curves and (b)AC impedance after introducing $FeMoO_4$ at various cycles(c)long-cycle test with $FeMoO_4$ and (d) amount of FeS/MoS_2 from profile-fitted peaks at various cycles

Figure 7(c) describes the effect of adding $FeMoO_4$ on the long-term stability of rGO-Fe_3O_4. The electrode was charged and discharged in 1M a Na_2SO_3 solution at a current density of 1.25 $A{\cdot}g^{-1}$ when 500mg $FeMoO_4$ was added into the electrolyte at the 780th cycle. The result shows a declining trend before adding $FeMoO_4$ and a reviving capacitance after 1000 cycles, with the capacitance reaching 238.87 $F{\cdot}g^{-1}$ by the end of 2250 cycles. The amount of FeS and MoS_2 were calculated by XRD fitting peak quantitative analysis (Figure 7d) at 500th, 1000th, 1500th and 2000th cycles, respectively. The mass fraction of FeS was 6.4%, 11.2%, 12.7% and 13.5% at 500th, 1000th ,1500th and 2000th cycle respectively, while the amount of MoS_2 was 0, 1.6%, 3.8% and 6.2% at corresponding cycle. Results indicate that the addition of $FeMoO_4$ hindered the growth of FeS, which confirms the inhibitory effect of growing MoS_2 on the formation of FeS and improving the specific capacitance in the long-term stability test.

Fe_3O_4 degradation mechanism

The behavior of the rGO-Fe_3O_4 electrode in sodium sulfite solution was explained by redox reactions on the surface (equations 2 and 3) [48]:

$$Fe_3O_4 + 4H_2O + 3S^{2-} + 2e^- \leftrightarrow 3FeS + 8OH^- \quad (4)$$

Equation 4 explains the degradation mechanism of Fe_3O_4-rGO composites during charge and discharge in the 1M Na_2SO_3 electrolyte, which is attributed to the growth of the FeS layer. According to the CV results obtained in Figure 3(a), the characteristic peak was caused by the conversion from Fe^{3+} to Fe^{2+}. Fe_3O_4 is converted into FeS, which is consistent with the sulfuration of Fe_3O_4 [49-51]. Due to the mutual attraction of the opposite charges, Fe^{2+} in the solution is distributed on the surface of the negatively charged rGO, thus reacting with S^{2-} and forming the FeS layer[52]. A schematic diagram of growing FeS on the electrode surface is shown in Figure 8.

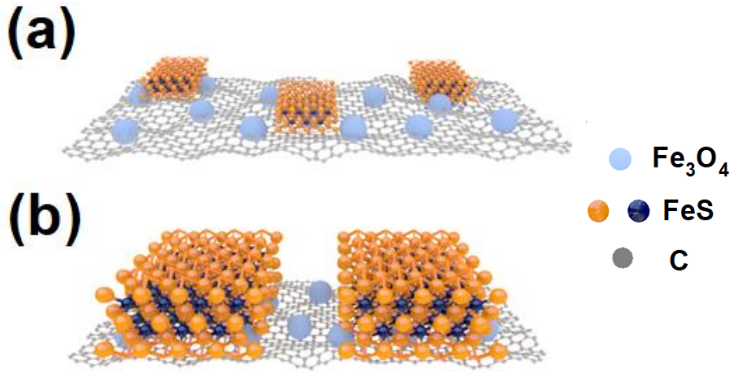

Figure 8 Schematic diagram of the process of FeS covering electrodes (a) after 50 cycles (b) partially covered.

It is worth noting that rGO-Fe_3O_4 composites provide a high capacity, however, it decreases as Fe_3O_4 inevitably undergoes irreversible redox reaction with sulfide ions in the solution (Equation 4) and finally forms FeS on the electrode surface through dissolution and recrystallization reactions during the charge and discharge cycles[53]. Despite that FeS derived from Fe_3O_4 has a relatively high theoretical capacity, significant changes in volume during the insertion/extraction of sodium ions lead to rapid loss of capacity. Hence, the formation of FeS on the electrode surface impedes the contact between Fe_3O_4 and the electrolyte[54-55]. As a result, A solid electrolyte interface(SEI) that inhibits redox reactions is formed on the electrode, thus preventing the Fe_3O_4 from exerting the pseudocapacitance effect and reducing the specific capacitance. On one hand, rGO contributes to stabilizing the electrode surface and improves cycling stability[56]. The oxygen-containing functional groups(like -*OH*) carried on rGO can increase surface wettability and provide additional pseudocapacitance[57]. On the other hand, the consumption of the electrolyte and the oxidation of the graphite also account for the capacitance loss over long-term charge and discharge process in which the oxygen content was increased in rGO. The possible redox reaction of rGO oxidation happened on electrode is presented [58-60]:

$$C-OH+H_2O \rightarrow C=O+H_3O^+ +e^- \quad (5)$$

Equation 5 explains the process by which the hydroxyl groups on the rGO surface interact with water to form anions and produce hydronium ions. In long-term charge/discharge cycles, the functional groups may react with the electrolyte or decompose, and the increase in the oxygen content of rGO may reduce the conductivity of the carbon electrode, resulting in low specific capacitance and poor rate performance[61-62]. The influence of rGO on the electrochemical performance of rGO-Fe_3O_4 and its degradation mechanism deserves more effort in the future study.

The increase in capacity performance by introducing the $FeMoO_4$ as an additive.

The chemical equilibrium in the solution when adding $FeMoO_4$ can be summarised as [63]:

$$[Fe^{2+}(Mo^{VI}O_4^{2-})_x] \leftrightarrow [Fe^{3+}(Mo^{VI}O_4^{2-})_{X-1}(Mo^{V}O_4^{3-})] \quad (6)$$

Fe(II) and Mo(VI) within the electrolyte are considered as soluble ions. Pseudocapacitor reactions of rGO-Fe_3O_4 involve the redox reaction of sulfur from sulfate and sulfite anions or the intercalation of sulfite ions for the redox reaction between Fe^{2+} and Fe^{3+}. The presence of the Mo element contributes to the formation of flaky MoS_2 through [64-65]:

$$S^{2-} + 2H_2O \leftrightarrow 2OH^- + H_2S \quad (7)$$

$$MoO_4^{2-} + 2e^- + 2H_2S \leftrightarrow MoS_2 + 4OH^- \quad (8)$$

The intermediate hydrogen sulfide reacts with molybdate ions under an aqueous environment to form the flaky MoS_2. The flaky MoS_2 covered electrode is electrically conductive, improving the electrical contact active area [66]. On the other hand, the consumption of sulfur ions (S^{2-}) inhibited the growth of FeS on the electrode surface and increased the capacity performance over long-term cycles.

The formation of flaky MoS_2 on the rGO-Fe_3O_4 composites in sodium sulfite solution can be generally classified into two stages, which is shown in Figure 9. The improvements in capacity performance by introducing $FeMoO_4$ can be attributed to two aspects. Unlike FeS, the formation of the porous MoS_2 layer with a gully morphology allows additional redox reactions, it is suggested that the formation of flaky MoS_2 with Fe_3O_4 was able to increase the electrical conductivity compared to that of pure Fe_3O_4 NPs. On the other hand, conductive MoS_2 provides an easy ion-diffusion path at electrode/electrolyte interface, which contributes to taking advantage of the electrochemical performance of rGO-Fe_3O_4 to the maximum extent. As a result, MoS_2 nanosheet generated on the electrode surface possessing a large surface area that provides abundant active Faraday redox reaction sites as well as facilitates electron transfer between electrode and electrolyte[67-69]. Meanwhile, the presence of MoS_2 effectively stabilizes the electrode/electrolyte interface and reinforces electrical conductivity[60]. These benefits could help to inhibit material degradation and slow down capacitance deterioration. Therefore, introducing $FeMoO_4$ can be concluded as an effective way to solve material degradation on rGO-Fe_3O_4 electrode surface in Na_2SO_3 environment under the test conditions. However, further work should be done on the investigation of the growth of MoS_2 and enhancement of the capacitance recovery within shorter periods.

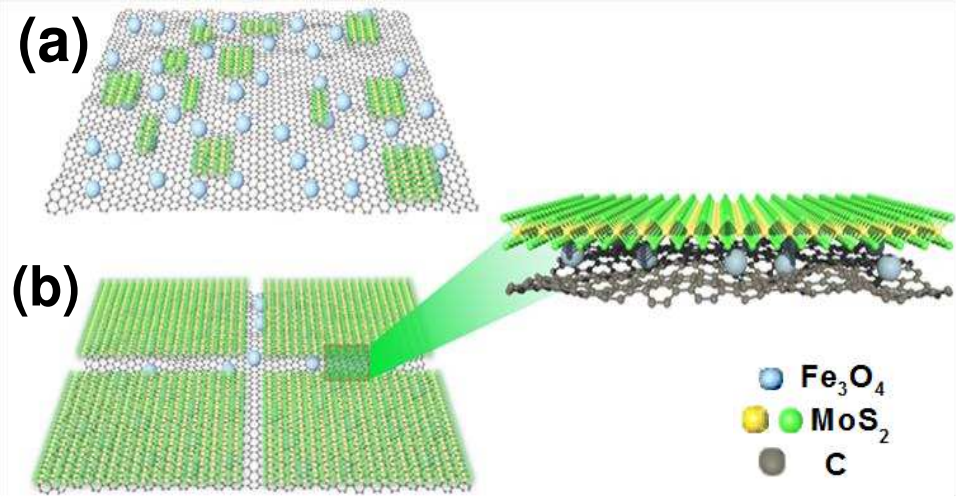

Figure 9. Schematic diagram of growing MoS_2 with rGO-Fe_3O_4 composites (a) partially covered and (b) fully covered

Conclusions

In summary, rGO-Fe_3O_4 composites were successfully synthesized by a hydrothermal method. Topographic and crystal characterization of XRD, SEM, Raman and TGA were used to confirm the formation of rGO-Fe_3O_4. As-prepared rGO-Fe_3O_4 composites show better electrochemical performance than pure Fe_3O_4, which proves the synergetic effect between Fe_3O_4 nanoparticles and rGO nanosheet. Capacitive properties of rGO-Fe_3O_4 were measured with cyclic voltammetry, GCD and impedance spectroscopy for electrodes with different rGO mass ratios. Enlarged specific surface area, high conductivity and low internal resistance facilitate electron transport effectively, thus improving the specific capacitance in Na_2SO_3 electrolyte. The sample with 1.5 $mg \cdot ml^{-1}$ rGO content exhibits the highest specific capacitance of 182.2 $F \cdot g^{-1}$ at a current density of 1.25 $A \cdot g^{-1}$ among prepared electrodes, with a retention rate of 92.4% after 1000 cycles. The degradation mechanism of rGO-Fe_3O_4 is based on the decrease in capacitance over long-term cyclic stability caused by the formation of FeS on the electrode surface and the oxidation of the carbon over long-term charge/discharge processes. Intentionally, $FeMoO_4$ was added as an additive to the electrolyte to inhibit capacitance decline. After adding $FeMoO_4$, MoS_2 was found on the electrode surface, thus providing additional sites for redox reaction, and assisting electron transfer. The maximum value of the specific capacitance was revived to 186.6 $F \cdot g^{-1}$, 171.8 $F \cdot g^{-1}$ and 153.4 $F \cdot g^{-1}$ at the current density of 1.25 $A \cdot g^{-1}$, 2.5 $A \cdot g^{-1,}$ and 3.75 $A \cdot g^{-1}$ after 500 cycles, respectively. Further, MoS_2 is found effectively in paving an easy and fast way for electron transfer and weakening the influence of FeS on deteriorating capacitance within a boundary condition of 2250 cycles. This work provides a new insight into improving the capacitive performance of rGO-Fe_3O_4 composites as well as preventing material degradation on the surface of the electrode.

Supporting Information

Supplementary material is attached in this section to further support research findings. These include a EDX mapping of FeS/MoS_2 products from the electrode surface, a SEM image of rGO-Fe_3O_4 composite and its corresponding EDX mapping.(pdf)

Reference

[1] Levitt A S, Alhabeb M, Hatter C B, Sarycheva A, Dion G, Gogotsi Y. Electrospun MXene/carbon nanofibers as supercapacitor electrodes. *Journal of Materials Chemistry A* **2019**, 7(1), 269-277. https://doi.org/10.1039/C8TA09810G

[2] Gomes V G. High-performance hybrid supercapacitor based on doped zucchini-derived carbon dots and graphene. *Materials Today Energy* **2019**, 12, 198-207. https://doi.org/10.1016/j.mtener.2019.01.013

[3] Zhang L, Lin H, Zhai L, Nie M, Zhou J, Zhuo S. Enhanced supercapacitor performance based on 3D porous graphene with MoO2 nanoparticles. *Journal of Materials Research* **2017**, 32(2), 292. https://doi.org/10.1557/jmr.2016.438

[4] Cui H, Huang W, Wu L, Cao S, Song, Y. Formation and electrochemical properties of petal-Like architectures derived from titanium alloy oxide nanotubes for supercapacitors. *Journal of Alloys and Compounds* **2019**, 785, 19-24. https://doi.org/10.1016/j.jallcom.2019.01.147

[5] Fan Y, Ma Z, Wang L, Dong Y, Jiang T, Li Z, Liu L, Shao G. In-situ synthesis of NiO foamed sheets on Ni foam as efficient cathode of battery-type supercapacitor. *Electrochimica Acta* **2018**, 269, 62-69. https://doi.org/10.1016/j.electacta.2018.02.141

[6] Zhang S, Shi X, Moszyński D, Tang T, Chu P.K, Chen X, Mijowska E. Hierarchical porous carbon materials from nanosized metal-organic complex for high-performance symmetrical supercapacitor. *Electrochimica Acta* **2018**, 269, 580-589. https://doi.org/10.1016/j.electacta.2018.03.043

[7] Zhou Q, Chen X, Su F, Lyu X, Miao, M. Sandwich-structured transition metal oxide/graphene/carbon nanotube composite yarn electrodes for flexible two-ply yarn supercapacitors. *Industrial & Engineering Chemistry Research* **2020**, 59(13), 5752-5759. https://doi.org/10.1021/acs.iecr.9b05524

[8] He X, Long X, Wang P, Wu H, Han P, Tang Y, Li K, Ma X, Zhang Y. Interconnected 3D Fe3O4/rGO as highly durable electrocatalyst for oxygen reduction reaction. *Journal of Alloys and Compounds* **2021**, 855, 157422. https://doi.org/10.1016/j.jallcom.2020.157422

[9] Wang Y, Huang S, Guo J, Ma Q, Shao Y, Chen K, Tang D. Effects of annealing holding time on capacitance performance of RuO2–IrO2–graphene/Ti electrodes. *Current Applied Physics* **2019**, 19(7), 835-841. https://doi.org/10.1016/j.cap.2019.04.017

[10] Ms N A D, Ms S N, Ms R B, Ms S R, W I S, P D D, Swain B. P. "Investigation of chemical bonding and supercapacitivity properties of Fe3O4-rGO nanocomposites for supercapacitor applications." *Diamond and Related Materials* **2020**, 104, 107756. https://doi.org/10.1016/j.diamond.2020.107756

[11] Ramanathan S, SasiKumar M, Radhika N, Obadiah A, Durairaj A, Swetha G. H, & Vasanthkumar, Santhoshkumar P, Lydia S, Vasanthkumara S. Musa paradisiaca reduced graphene oxide (BRGO)/MWCNT-Fe3O4 nanocomposite for supercapacitor and photocatalytic applications. *Materials Today*: Proceedings **2021**. https://doi.org/10.1016/j.matpr.2021.01.706

[12] Wang X, Jiang D, Jing C, Liu X, Li K, Yu M, Qi S, Zhang, Y. Biotemplate Synthesis of Fe3O4/Polyaniline for Supercapacitor. *Journal of Energy Storage* 2020, 30, 101554. https://doi.org/10.1016/j.est.2020.101554

[13] Pal B, Yang S, Ramesh S, Thangadurai V, Jose R. Electrolyte selection for supercapacitive devices: a critical review. *Nanoscale Advances* **2019**, 1(10), 3807-3835.. https://doi.org/10.1039/C9NA00374F

[14] Huang J, Fan L, Gu Y, Geng C, Luo H, Huang Y, Lin J, Wu, J. One-step solvothermal synthesis of high-capacity Fe3O4/reduced graphene oxide composite for use in Li-ion capacitor. *Journal of Alloys and Compounds* **2019**, 788, 1119-1126. https://doi.org/10.1016/j.jallcom.2019.03.004

[15] Fic K, He M. L, Berg E, Novak P, Frackowiak E. Comparative operando study of degradation mechanisms in carbon-based electrochemical capacitors with Li_2SO_4 and $LiNO_3$ electrolytes. *Carbon* **2017**, 120, 281-293. https://doi.org/10.1016/j.carbon.2017.05.061

[16] Tokita M, Yoshimoto N, Fujii K, Morita M. Masahiro Degradation Characteristics of Electric Double-Layer Capacitors Consisting of High Surface Area Carbon Electrodes with Organic Electrolyte Solutions. *Electrochimica Acta* **2016**, 209, 210-218. https://doi.org/10.1016/S0167-2738(98)00280-X

[17] Javed M. S., Khan A. J., Hanif M., Nazir M. T., Hussain S., Saleem M., Raza R, Yun S, Liu Z. Engineering the performance of negative electrode for supercapacitor by polyaniline coated Fe3O4 nanoparticles enables high stability up to 25,000 cycles. International *Journal of Hydrogen Energy* **2021**, 46(15), 9976-9987. https://doi.org/10.1016/j.ijhydene.2020.04.173

[18] Abbas Q, Ratajczak P, Béguin F. Sodium molybdate–an additive of choice for enhancing the performance of AC/AC electrochemical capacitors in a salt aqueous electrolyte, *Faraday discussions*, **2014**, 172: 199-214. https://doi.org/10.1039/C4FD00056K

[19] Chodankar N R, Dubal D P, Lokhande A C, Patil A. M, Kim J. H., Lokhande, C. D. An innovative concept of use of redox-active electrolyte in asymmetric capacitor based on MWCNTs/MnO2 and Fe2O3 thin films. *Scientific reports* **2016**, 6(1): 1-14. https://doi.org/10.1038/srep39205

[20] Zhang M, Wang G, Lu L, Wang T, Xu H, Yu C, Li H, Tian, W. Improving the electrochemical performances of active carbon-based supercapacitors through the combination of introducing functional groups and using redox additive electrolyte. *Journal of Saudi Chemical Society* **2018**, 22(8), 908-918. https://doi.org/10.1016/j.jscs.2018.02.001

[21] Ma Y, Hou C, Zhang H, Zhang Q, Liu H, Wu S, Guo Z. Three-dimensional core-shell Fe_3O_4/Polyaniline coaxial heterogeneous nanonets: Preparation and high performance supercapacitor electrodes. *Electrochimica Acta* **2019**, 315, 114-123. https://doi.org/10.1016/j.electacta.2019.05.073

[22] Padhi D. K., Panigrahi T. K, Parida K, Singh S. K., Mishra P. M. Green synthesis of Fe3O4/RGO nanocomposite with enhanced photocatalytic performance for Cr (VI) reduction, phenol degradation, and antibacterial activity. *ACS Sustainable Chemistry & Engineering* **2017**, 5(11), 10551-10562. https://doi.org/10.1021/acssuschemeng.7b02548

[23] Liang C L, Liu Y, Bao R, Luo Y, Yang W, Xie B, Yang M. Effects of Fe3O4 loading on the cycling performance of Fe3O4/rGO composite anode material for lithium ion batteries. *Journal of Alloys and Compounds* **2016**, 678, 80-86. https://doi.org/10.1016/j.jallcom.2016.03.274

[24] Ding R, Zhang J, Qi J, Li Z, Wang C, Chen, M. N-doped dual carbon-confined 3D architecture rGO/Fe3O4/AC nanocomposite for high-performance lithium-ion batteries. *ACS applied materials & interfaces* **2018**, 10(16), 13470-13478.

https://doi.org/10.1021/acsami.8b00353

[25] Natarajan S, Ede S. R, Bajaj H. C, Kundu, S. Environmental benign synthesis of reduced graphene oxide (rGO) from spent lithium-ion batteries (LIBs) graphite and its application in supercapacitor. *Colloids and Surfaces A: Physicochemical and Engineering Aspects* **2018**, 543, 98-108. https://doi.org/10.1016/j.colsurfa.2018.01.054

[26] Sheng S, Liu W, Zhu K, Cheng K, Ye K, Wang G, Cao D, Yan, J. Fe3O4 nanospheres in situ decorated graphene as high-performance anode for asymmetric supercapacitor with impressive energy density. *Journal of colloid and interface science* **2019**, 536, 235-244. https://doi.org/10.1016/j.jcis.2018.10.060

[27] Wang Q, Jiao L, Du H, Wang Y, Yuan H. Fe3O4 nanoparticles grown on graphene as advanced electrode materials for supercapacitors. *Journal of Power Sources* **2014**, 245, 101-106. https://doi.org/10.1016/j.jpowsour.2013.06.035

[28] Zhang S, Li C, Zhang X, Sun X, Wang K, Ma Y. High performance lithium-ion hybrid capacitors employing Fe3O4–graphene composite anode and activated carbon cathode. *ACS applied materials & interfaces* **2017**, 9(20), 17136-17144. https://doi.org/10.1021/acsami.7b03452

[29] Ghaly H. A, El-Deen A. G, Souaya E. R, Allam N. K. Asymmetric supercapacitors based on 3D graphene-wrapped V2O5 nanospheres and Fe3O4@ 3D graphene electrodes with high power and energy densities. *Electrochimica Acta* **2019**, 310, 58-69. https://doi.org/10.1016/j.electacta.2019.04.071

[30] Zhou Y, Zhao X, Liu F, Chi W, Yao J, Chen G. Facile One-Pot Solvothermal Synthesis of the RGO/MWCNT/Fe3O4 Hybrids for Microwave Absorption. *ACS omega* **2020**, 5(6), 2899-2909. https://doi.org/10.1021/acsomega.9b03740

[31] Basavegowda N, Mishra K, Lee, Y. R. Fe3O4-decorated MWCNTs as an efficient and sustainable heterogeneous nanocatalyst for the synthesis of polyfunctionalised pyridines in water. *Materials Technology* **2019**, 34(9), 558-569. https://doi.org/10.1080/10667857.2019.1593291

[32] Fan X, Jiao G, Gao L, Jin P, Li X. The preparation and drug delivery of a graphene–carbon nanotube–Fe3O4 nanoparticle hybrid. *Journal of Materials Chemistry B* **2013**, 1(20), 2658-2664. https://doi.org/10.1039/c3tb00493g

[33] Xin, B, Zeng H, Huang G, Jia J, Yuan R, Zhang C, Sun Q, Cao Y, Chen Z, Liu, B. Magnesium citrate induced growth of noodle-like porous graphitic carbons from coal tar pitch for high-performance lithium-ion batteries. *Electrochimica Acta* **2021**, 138043. https://doi.org/10.1016/j.electacta.2021.138043

[34] Wang Z, Xing B, Zeng H, Huang G, Liu X, Guo H, Zhang C, Cao Y, Chen Z. Space-confined carbonization strategy for synthesis of carbon nanosheets from glucose and coal tar pitch for high-performance lithium-ion batteries. *Applied Surface Science* **2021**, 547, 149228. https://doi.org/10.1016/j.apsusc.2021.149228

[35] Xing B, Zhang C, Liu Q, Zhang C, Huang G, Guo H, Cao Z, Cao Y, Yu J, Chen, Z. Green synthesis of porous graphitic carbons from coal tar pitch templated by nano-CaCO3 for high-performance lithium-ion batteries. *Journal of Alloys and Compounds* **2019**, 795, 91-102. https://doi.org/10.1016/j.jallcom.2019.04.300

[36] Kumar M. P, Lathika L. M, Mohanachandran A. P, Rakhi, R. B. A High-Performance

Flexible Supercapacitor Anode Based On Polyaniline/Fe3O4 Composite@ Carbon Cloth. *ChemistrySelect* **2018**, 3(11), 3234-3240. https://doi.org/10.1002/slct.201800305

[37] Zhang K, Zhang Q, Gao X, Chen X, Wang Y, Li W, Wu J. Effect of absorbers' composition on the microwave absorbing performance of hollow Fe3O4 nanoparticles decorated CNTs/graphene/C composites. *Journal of Alloys and Compounds* **2018**, 748, 706-716. https://doi.org/10.1016/j.jallcom.2018.03.202

[38] Misnon I. I, Abd Aziz R, Zain N. K. M, Vidhyadharan B, Krishnan S. G, Jose, R. High performance MnO2 nanoflower electrode and the relationship between solvated ion size and specific capacitance in highly conductive electrolytes. *Materials Research Bulletin* **2014**, 57, 221-230. https://doi.org/10.1016/j.materresbull.2014.05.044

[39] Zhao X, Johnston C, Crossley A, Grant, P. S. Printable magnetite and pyrrole treated magnetite based electrodes for supercapacitors. *Journal of Materials Chemistry* **2020**, 20(36), 7637-7644. https://doi.org/10.1039/C0JM00028K

[40] Wang S. Y, Ho K. C, Kuo S. L, Wu, N. L. Investigation on capacitance mechanisms of Fe3O4 electrochemical capacitors. *Journal of the Electrochemical Society* **2005**, 153(1), A75. https://doi.org/ 10.1149/1.2131820

[41] Ma Y, Hou C, Zhang H, Zhang Q, Liu H, Wu S, Guo, Z. Three-dimensional core-shell Fe3O4/Polyaniline coaxial heterogeneous nanonets: Preparation and high performance supercapacitor electrodes. *Electrochimica Acta* **2019**, 315, 114-123. https://doi.org/10.1016/j.electacta.2019.05.073

[42] Zhao X, Jia Y, Liu, Z. H. GO-graphene ink-derived hierarchical 3D-graphene architecture supported Fe3O4 nanodots as high-performance electrodes for lithium/sodium storage and supercapacitors. *Journal of colloid and interface science* **2019**, 536, 463-473. https://doi.org/10.1016/j.jcis.2018.10.071

[43] Shao Y, Feng K, Zhang S, Zhang R, He S, Wei X, Lin Y, Ye Z, Chen, K. IrO2–CeO2-graphene/Ti porous electrode with high charge-transfer speed and enhanced capacitance. *Ceramics International* **2021**, 47(3), 3728-3740. https://doi.org/10.1016/j.ceramint.2020.09.230

[44] Chen Y, Tian G, Shi Y, Xiao Y, Fu, H. Hierarchical MoS2/Bi2MoO6 composites with synergistic effect for enhanced visible photocatalytic activity. *Applied Catalysis B: Environmental* **2015**, 164, 40-47. https://doi.org/10.1016/j.apcatb.2014.08.036

[45] Robinson B. J, Giusca C. E, Gonzale, Y. T, Kay N. D, Kazakova O, Kolosov, O. V. Structural, optical and electrostatic properties of single and few-layers MoS2: effect of substrate. *2D Materials* **2015**, 2(1), 015005. https://doi.org/10.1088/2053-1583/2/1/015005

[46] Lee C, Yan H, Brus L. E, Heinz T. F, Hone J, Ryu, S. Anomalous lattice vibrations of single-and few-layer MoS2. *ACS nano* **2010**, 4(5), 2695-2700. https://doi.org/10.1021/nn1003937

[47] Bissett M. A, Kinloch I. A, Dryfe, R. A. Characterization of MoS2–graphene composites for high-performance coin cell supercapacitors. *ACS applied materials & interfaces* **2015** 7(31), 17388-17398. https://doi.org/10.1021/acsami.5b04672

[48] Nithya V. D, Arul N. S. Progress and development of Fe 3 O 4 electrodes for supercapacitors. *Journal of Materials Chemistry A* **2016**, 4(28), 10767-10778. https://doi.org/10.1039/C6TA02582J

[49] Beyazay T, Oztuna F. E. S, Unal O, Acar H. Y, Unal, U. Free-Standing N-doped Reduced

Graphene Oxide Papers Decorated with Iron Oxide Nanoparticles: Stable Supercapacitor Electrodes. *ChemElectroChem* **2016**, 6(14), 3774-3781. https://doi.org/10.1002/celc.201900855

[50] Lee S. Y, Kang, Y. C. Sodium‐Ion Storage Properties of FeS–Reduced Graphene Oxide Composite Powder with a Crumpled Structure. *Chemistry–A European Journal* **2016**, 22(8), 2769-2774. https://doi.org/10.1002/chem.201504579

[51] Yu L, Yang B, Liu Q, Liu J, Wang X, Song D, Wang, J, Jing, X. Interconnected NiS nanosheets supported by nickel foam: soaking fabrication and supercapacitors application. *Journal of Electroanalytical Chemistry* **2015**, 739, 156-163. https://doi.org/10.1016/j.jelechem.2014.12.031

[52] Shao X, Zhu Z, Zhao C, Zhao C, Qian X. Hierarchical FeS/RGO/FeS@ Fe foil as high-performance negative electrode for asymmetric supercapacitors. *Inorganic Chemistry Frontiers* **2018**, 5(8), 1912-1922. https://doi.org/10.1039/C8QI00227D

[53] Shangguan E, Li F, Li J, Chang Z, Li Q, Yuan X. Z, Wang, H. FeS/C composite as high-performance anode material for alkaline nickel–iron rechargeable batteries. *Journal of Power Sources* **2015**, 291, 29-39. https://doi.org/10.1016/j.jpowsour.2015.05.019

[54] Hou B. H, Wang Y. Y, Guo J. Z, Zhang Y, Ning Q. L, Yang Y, Li, W. H, Zhang J. P, Wang X. L, Wu, X. L. A scalable strategy to develop advanced anode for sodium-ion batteries: commercial Fe3O4-derived Fe3O4@ FeS with superior full-cell performance. *ACS applied materials & interfaces* **2018**, 10(4), 3581-3589. https://doi.org/10.1021/acsami.7b16580

[55] Rubio S, Maça R. R, Ortiz G. F, Vicente C. P, Lavela P, Etacheri V, Tirado J. L. Iron Oxide–Iron Sulfide Hybrid Nanosheets as High-Performance Conversion-Type Anodes for Sodium-Ion Batteries. *ACS Applied Energy Materials* **2020**, 3(11), 10765-10775. https://doi.org/10.1021/acsaem.0c01814

[56] Krishnan S. G, Harilal M, Yar A, Vijayan B. L, Dennis J. O, Yusoff M. M, Jose, R. Critical influence of reduced graphene oxide mediated binding of M (M= Mg, Mn) with Co ions, chemical stability and charge storability enhancements of spinal-type hierarchical MCo2O4 nanostructures. *Electrochimica Acta* **2017**, 243, 119-128. https://doi.org/10.1016/j.electacta.2017.05.064

[57] Zhao Y, Ran W, He J, Song Y, Zhang C, Xion, D. B, Gao F, Wu J, Xia, Y. Oxygen-rich hierarchical porous carbon derived from artemia cyst shells with superior electrochemical performance. *ACS applied materials & interfaces,* **2015** 7(2), 1132-1139. https://doi.org/10.1021/am506815f

[58] Fang Y, Luo B, Jia Y, Li X, Wang B, Song Q, Kang F, Zhi, L. Renewing functionalized graphene as electrodes for high‐performance supercapacitors. *Advanced materials* **2012**, 24(47), 6348-6355. https://doi.org/10.1002/adma.201202774

[59] Krishnan P, Biju V. Reduced graphite oxide-pure water supercapacitor: A futuristic water based energy storage device. *Physica E: Low-dimensional Systems and Nanostructures* **2021**, 126, 114452. https://doi.org/10.1016/j.physe.2020.114452

[60] Liu Y, Huang G, Li Y, Yao Y, Liu Q, Xing B, Jia J, Zhang, C. Structural evolution of porous graphitic carbon nanosheets based on quinonyl decomposition for supercapacitor electrodes. *Applied Surface Science* **2021**, 537, 147824. https://doi.org/10.1016/j.apsusc.2020.147824

[61] Singh K. P, Song M. Y, Yu J. S. Iodine-treated heteroatom-doped carbon: conductivity

driven electrocatalytic activity. *Journal of Materials Chemistry A* **2014**, 2(42), 18115-18124. https://doi.org/10.1039/C4TA03706E

[62] Yang W, Yang W, Song A, Gao L, Su L, Shao, G. Supercapacitance of nitrogen-sulfur-oxygen co-doped 3D hierarchical porous carbon in aqueous and organic electrolyte. *Journal of Power Sources* **2017**, 359, 556-567. https://doi.org/10.1016/j.jpowsour.2017.05.108

[63] Nikolenko N. V, Kozhevnikov I. V, Kostyniuk A. O, Bayahia H, Kalashnykov, Y. V. Preparation of iron molybdate catalysts for methanol to formaldehyde oxidation based on ammonium molybdoferrate (II) precursor. *Journal of Saudi Chemical Society* **2018**, 22(3), 372-379. https://doi.org/10.1016/j.jscs.2016.04.002

[64] Karade S. S, Dubal D. P, Sankapal, B. R. MoS 2 ultrathin nanoflakes for high performance supercapacitors: room temperature chemical bath deposition (CBD). *RSC advances* **2016**, 6(45), 39159-39165. http://dx.doi.org/10.1039/C6RA04441G

[65] Ding X, Huang Y, Li S, Zhang N, Wang, J. 3D architecture reduced graphene oxide-MoS2 composite: preparation and excellent electromagnetic wave absorption performance. *Composites Part A: Applied Science and Manufacturing* **2016**, 90, 424-432. https://doi.org/10.1016/j.compositesa.2016.08.006

[66] Liu C, Wang L, Tang Y, Luo S, Liu Y, Zhang S, Zeng Y, Xu, Y. Vertical single or few-layer MoS2 nanosheets rooting into TiO2 nanofibers for highly efficient photocatalytic hydrogen evolution. *Applied Catalysis B: Environmental* **2015**, 164, 1-9. https://doi.org/10.1016/j.apcatb.2014.08.046

[67] Shi Z, Zhu J, Li Z, Xiao Q, Zhu, J. Sulfur-Doped Nickel–Cobalt Double Hydroxide Electrodes for High-Performance Asymmetric Supercapacitors. *ACS Applied Energy Materials* **2020**, 3(11), 11082-11090. https://doi.org/10.1021/acsaem.0c02058

[68] Kumar R, Singh R. K, Vaz A. R, Savu R, Moshkalev, S. A. Self-assembled and one-step synthesis of interconnected 3D network of Fe3O4/reduced graphene oxide nanosheets hybrid for high-performance supercapacitor electrode. *ACS applied materials & interfaces* **2017**, 9(10), 8880-8890. https://doi.org/10.1021/acsami.6b14704

[69] Barik R, Raulo A, Jha S, Nandan B, Ingole P. P. Polymer-Derived Electrospun Co3O4@ C Porous Nanofiber Network for Flexible, High-Performance, and Stable Supercapacitors. *ACS Applied Energy Materials* **2020**, 3(11), 11002-11014. https://doi.org/10.1021/acsaem.0c01955

[70] Hu H, Zhong X, Yang S, Fu, H. Tough and stretchable Fe3O4/MoS2/PAni composite hydrogels with conductive and magnetic properties. *Composites Part B: Engineering* **2020**, 182, 107623. https://doi.org/10.1016/j.compositesb.2019.107623